

SOLUBILITIES AND DIFFUSION OF TRACE GASES IN COLD SULFURIC ACID FILMS

Stefan Langenberg

*Institut für Physikalische und Theoretische Chemie, University of Bonn,
Wegelerstr. 12, D-53115 Bonn, Germany*

Volker Proksch and Ulrich Schurath

*Institut für Meteorologie und Klimaforschung, Forschungszentrum Karlsruhe
GmbH, P.O. Box 3640, D-76021 Karlsruhe, Germany*

The well known technique of gas chromatography was used to determine solubilities and liquid phase diffusion coefficients of trace gases in a thin sulfuric acid film deposited in a fused silica column. Solubilities of SO_2 , NO_2 , and N_2O_4 and the diffusion coefficient of SO_2 were measured in the temperature range 203 - 243 K using sulfuric acid concentrations in the range of 39–83wt%. The results suggest that sulfuric acid aerosol particles are not a physical sink for these trace gases.

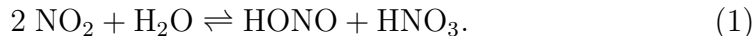
Key words: Henry's law, sulfur dioxide, nitrogen dioxide, dinitrogen tetroxide, aerosol

1 Introduction

Current interest in solubilities and liquid phase diffusion coefficients of trace gases in cold sulfuric acid solutions arises from the potential importance of heterogeneous processes which occur in sulfuric acid droplet aerosols in the upper troposphere and lower stratosphere, e.g. (Zhang et al. 1996). Sulfuric acid also forms in contrails of aircraft (Kärcher et al. 1995), condensing on simultaneously emitted soot particles and/or creating new nanodroplets by homogeneous bimolecular nucleation with water vapour, followed perhaps by uptake of HNO_3 and more water vapour and eventually by freezing, until a visible contrail is formed (Kärcher 1996; Kärcher et al. 1996; Schumann et al. 1996). Important trace gases which are emitted by aircraft and thus might dissolve/react in the sulfuric acid droplets or in liquid acid coatings of soot

particles are SO_2 and NO_x . Most NO_x is emitted as NO which is, however, rapidly oxidized to NO_2 as the exhaust gases mix with ozone-rich ambient air.

We have measured the solubilities of SO_2 , and of NO_2 in equilibrium with its dimer N_2O_4 , in very thin cold sulfuric acid films at concentrations and temperatures covering conditions in the mid and upper troposphere and in the lower stratosphere. Diffusion coefficients of SO_2 in cold sulfuric acid were also obtained. The reaction of NO_2 with sulfuric acid is considered to be a source of nitrous acid in the atmosphere (Wiesen et al. 1995):



Gaseous HONO absorbs solar uv radiation of $\lambda < 390$ nm, and photodissociates with a quantum yield of unity at an approximate rate of $1.5 \times 10^{-3} \text{ s}^{-1}$ in bright sunlight (Bongartz et al. 1991). This makes the compound an important OH source in NO_x -polluted ozone-depleted air masses. In very concentrated sulfuric acid, the nitrosonium cation NO^+ is formed from HONO:



NO^+ and HONO may play key roles in an alternative chlorine activation mechanism which leads to the formation of ClNO by their reactions with HCl (Zhang et al. 1996; Fenter and Rossi 1996).

In order to understand and quantify the formation of HONO from NO_2 in sulfuric acid droplets or on particulate matter coated with a sulfuric acid film, the solubilities of the reactants and products must be known in the relevant temperature range. While the solubility of HONO in cold sulfuric acid has recently been measured (Becker et al. 1996), nothing is known about the solubility of NO_2 and its more reactive dimer, N_2O_4 , which is the likely precursor of HONO in solution. A simple capillary GC technique was adopted in this work, using thin cold sulfuric acid films as stationary phase, to determine solubilities and diffusion coefficients in the liquid coating on the basis of retention time and peak broadening theories, and to study reactions in solution.

2 Experimental

All experiments were carried out using capillary GC wide bore columns (fused silica, $l = 2.8$ m, $\text{Ø} 530 \mu\text{m}$) internally coated with sulfuric acid (film thickness $h = 1 - 2 \mu\text{m}$). The columns, which were immersed in the cold liquid of a bath cryo-thermostat with a useful temperature range $T \geq 193$ K regulated to ± 0.1 K, were operated like ordinary GC columns with an inert carrier gas

(synthetic air). The carrier gas flow rate could be varied by means of a mass flow controller (MKS, range 0-20 sccm), while the column head pressure was monitored by a pressure transducer. Dilute trace gases were injected either manually through a silicone rubber septum, or by means of a computer controlled six port valve. Retention times and peak shapes of the trace gases were determined with suitable fast response trace gas detectors.

Empty fused silica columns were coated with sulfuric acid films by a dynamic coating technique (Redant et al. 1982): a pre-column of 2 m length, filled with a sulfuric acid solution of the desired concentration, was connected with the empty column to be coated. The liquid acid plug was pushed through the empty column under regulated gas pressure, and trapped in a post column of the same inner diameter and suitable length to maintain a constant plug speed v until the entire column was coated. When plain sulfuric acid solutions were utilized, the obtained coatings were unstable, breaking up immediately to form small beads on the tube wall. This is attributed to the large surface tension of the acid and the poor wettability of the neat silica surface. We found, however, that stable sulfuric acid films could be prepared by adding a suitable surfactant to the acid. Best results were achieved when 3 mM of the surfactant Nonidet-P40 (ethylenphenolpoly-(ethylenglycoether) $_n$, $n = 11$) were admixed to the acid.

The film thickness h obtained by the dynamic coating technique depends on the column radius r , the plug speed v , the viscosity η of the acid, and its surface tension γ (Guiochon 1971):

$$h \approx 1.34r \left(\frac{v\eta}{\gamma} \right)^{2/3}. \quad (3)$$

Although viscosities η of sulfuric acid have recently been measured as a function of concentration and temperature (Williams and Long 1995), this equation can only yield an estimate of the expected film thickness since the surface tension γ of the acid is reduced by the surfactant. To determine the true film thickness which must be known to analyse the experimental results, columns were rinsed with a few ml of Milli-Q water after each series of measurements, and the mass m_l of acid titrated with 0.01 N NaOH. The film thickness was calculated from m_l and the known density of the acid film (Carslaw et al. 1995). When a column was coated with 68wt% H₂SO₄ using a plug speed of $1.8 \times 10^{-3} \text{ m s}^{-1}$, a film of $1.8 \text{ }\mu\text{m}$ thickness was obtained. Equation (3) then yields an effective surface tension $\gamma = 0.04 \text{ N m}^{-1}$, which can be compared with the reported surface tension $\gamma = 0.076 \text{ N m}^{-1}$ of detergent-free acid of the same concentration (Sabinina and Terpugow 1935).

The variability of the film thickness along the column was also investigated by cutting a coated column in pieces of about 10 cm length. Each piece was

rinsed with 20 ml Milli-Q water which was subsequently analysed by ion chromatography. A film thickness variability of $\pm 8\%$ was found for this column.

During the experiments the acid film loses water by evaporation. Therefore the sulfuric acid concentration in the liquid film increases. Assuming a mass-flow \dot{n} ($[\dot{n}] = \text{mol s}^{-1}$) of completely dry carrier gas into the column and uniform evaporation of water along the column, the concentration change of the sulfuric acid in terms of weight fraction w is given by

$$\frac{dw}{dt} = \frac{M(\text{H}_2\text{O})}{m_l} \frac{p(\text{H}_2\text{O})}{p_o} \dot{n}, \quad (4)$$

depending on the partial pressure $p(\text{H}_2\text{O})$ which is very low at the experimental temperatures, and on the pressure p_o at column exit. A maximum total concentration change of 2wt% was estimated for a series of experiments carried out with a 39wt% sulfuric acid film. More concentrated sulfuric acid films are even more stable.

The SO_2 experiments were carried out by manually injecting 20 - 500 μl samples of 200 - 800 ppm SO_2 and 8 ppm SF_6 in synthetic air with a gas-tight syringe. The SF_6 was added as an insoluble tracer to determine the system void time. A modified Bendix flame photometric sulphur monitor was used as a GC detector. The photomultiplier anode current was amplified and fed into a computer, which converted the signal to sulfur mass flow using a non-linear calibration curve.

Interactions of NO_2 with the cold sulfuric acid film were studied by injecting 1 - 400 ppm NO_2 in nitrogen from a permeation source, using a 6-port valve with a 100 μl sampling loop. NO_2 peaks were measured as NO with a laboratory-built fast responding chemiluminescence analyser preceded by a thermal converter. The converter, which consisted of a gold wire in a thin quartz tube heated to 540 K, was run with 0.3% methanol vapour instead of the more commonly used CO reagent (Nyarady et al. 1985). This eliminated poisoning of the gold wire which occurs when metal carbonyl impurities are present in the CO gas. Detector calibrations and determinations of column void times t_0 at each column temperature were carried out by injecting of 5.1 ppm NO in N_2 (Messer Griesheim). To make sure that NO did not react with the cold sulfuric acid film, injections of a fixed amount of NO were repeated for a wide range of carrier gas flow rates: the amount of NO eluted from the column turned out to be independent of the column residence time, and no net retention of the trace gas was observed.

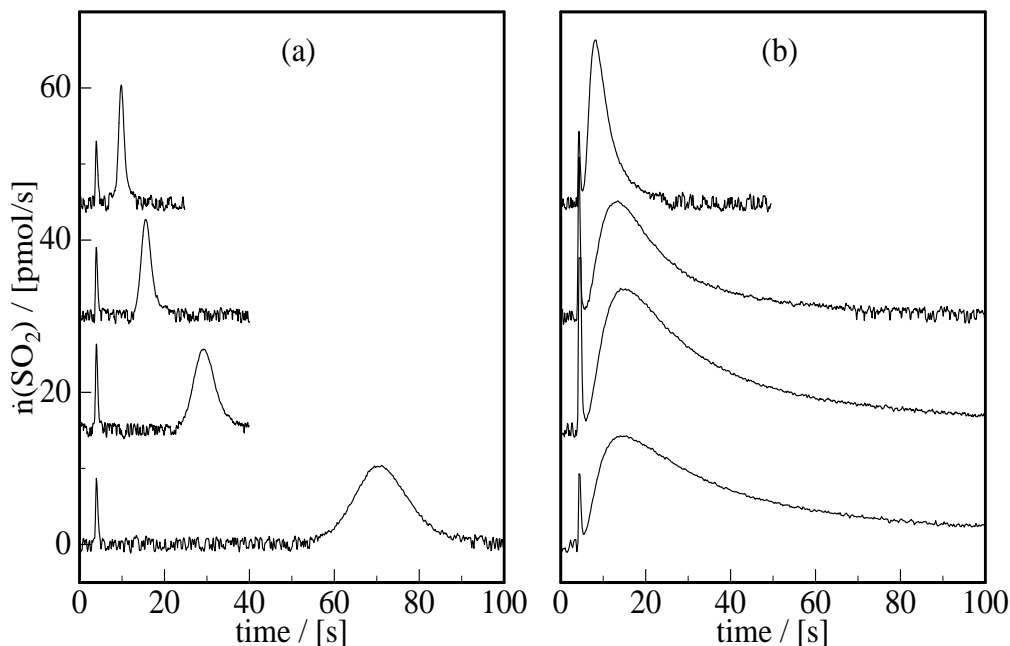


Fig. 1. Series of chromatograms of SF_6/SO_2 at 20 ml min^{-1} at 243, 233, 223, and 213 K. Acid (a) 41wt%, film thickness $1.2 \mu\text{m}$; (b) 83wt%, film thickness $2.1 \mu\text{m}$

3 Results and Discussion

3.1 Solubility and Diffusion of SO_2

Because SO_2 is a weak acid in water, it is only physically dissolved in sulfuric acid. As the peak is swept through the acid-coated column by the carrier gas, SO_2 is first dissolved and then re-evaporated from the liquid acid film. If the acid film is sufficiently thin, Henry's law equilibrium will be locally established along the column to a good approximation. Under such conditions the capacity ratio k' can be determined from the adjusted retention time t_n of the eluting SO_2 peak, which is a known function of Henry's law constant (Giddings 1991):

$$k' = \frac{n_l}{n_g} = \frac{t_n}{t_0} = \frac{m_l H R T}{\pi r^2 l} \quad (5)$$

The capacity ratio equals the ratio of the amounts of SO_2 in the liquid (n_l) and the gas phase (n_g) in the column. The adjusted retention time is determined from $t_n = t_r(\text{SO}_2) - t_r(\text{SF}_6)$, noting that SF_6 does not dissolve in the acid film, and thus is not retained. The column void time is related to the carrier gas mass flow rate \dot{n} ,

$$t_0 = \frac{\pi r^2 l p_o}{\dot{n} R T j}, \quad (6)$$

where j is the James-Martin correction factor (Giddings 1991) which takes into account the compressibility of the carrier gas. Combining these expressions yields

$$H = \frac{\pi r^2 l}{m_l RT} k' = \frac{\dot{n} j t_n}{m_l p_o}. \quad (7)$$

($[H] = \text{mol kg}^{-1} \text{bar}^{-1}$). These simple relations are valid for Gaussian-shaped peaks, while the observed peaks were only approximately Gaussian-shaped, see Fig. 1. The peaks deviate from the Gaussian shape because unlike in normal gas chromatography the time needed to saturate the stationary phase is only moderately shorter than the time the peak needs to pass through the column. To retain the simple theory, exponentially modified Gauss functions (Goodman and Brenna 1994) were fitted to the SO_2 peaks, yielding retention times $t_r(\text{SO}_2)$ and second central moments σ^2 of the peaks.

To check for the local equilibrium assumption underlying equation (7), the carrier gas flow rate was varied at each column temperature, and the corresponding ratios t_n/t_0 were plotted against the carrier gas velocity u . At higher temperatures the ratios t_n/t_0 were indeed independent of u , showing that equation (5) was valid. However, at very low temperatures and high sulfuric acid concentrations, t_n/t_0 became a function of u . At these temperatures an estimate of the true capacity ratio k' , to be used in equation (5), was obtained by plotting t_n/t_0 versus the flow rate u , and extrapolating the plot to $u = 0$. The uncertainty in the extrapolated capacity ratios k' , which was of the order of 10%, contributes the largest error to Henry's law constants H determined by the capillary column method.

Semilog plots of the obtained Henry's law constants H versus $1/T$ are shown in Fig. 2. Hypothetical Henry's law constants of SO_2 in supercooled water are included for comparison. They were calculated using thermodynamic constants derived from solubility data in the 278-393 K range, as recommended by Goldberg and Parker (1985). The lowering of the solubility in sulfuric acid solutions, as compared with pure supercooled water, can be explained by the salting out effect.

Note that the thermodynamic freezing points of aqueous sulfuric acid are $T_f(41\text{wt}\%) = 217 \text{ K}$; $T_f(62\text{wt}\%) = 240 \text{ K}$; $T_f(83\text{wt}\%) = 281 \text{ K}$ (Gable et al. 1950), significantly higher than the lower limit of the temperature range studied in this work. Hence, film freezing might have occurred in our experiments. This should have given rise to irregularities in the T -dependencies of the solubilities, and accordingly in the plots of $\ln H$ versus $1/T$, Fig. 2. With the exception of two data points at the highest acid concentrations and lowest temperatures, no such discontinuities were observed, indicating that the sulfuric acid films remained supercooled liquid. This is consistent with infrared

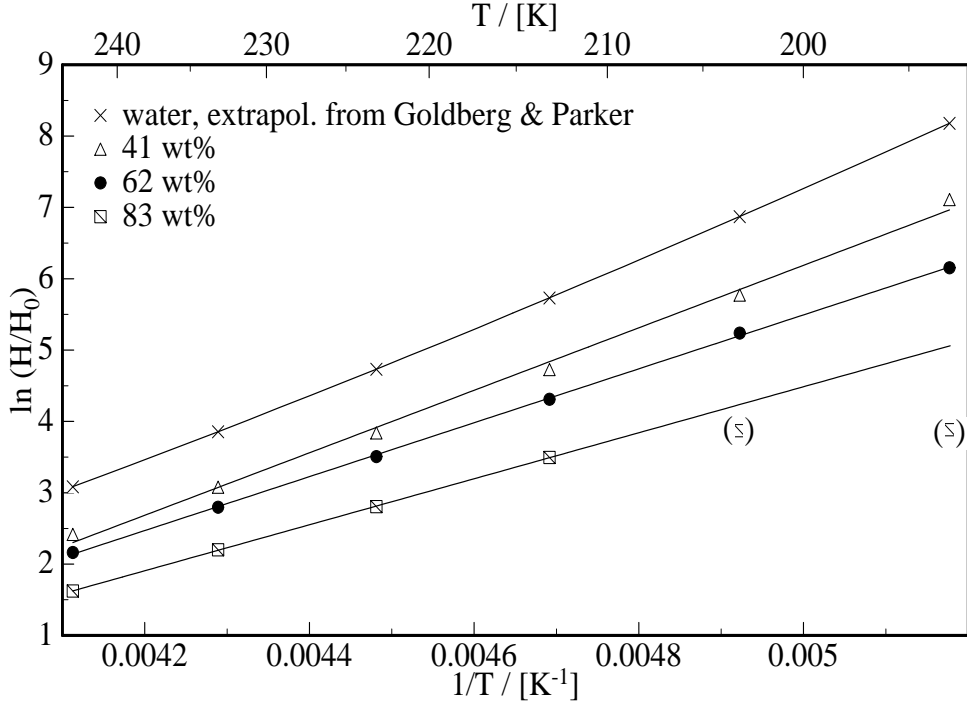


Fig. 2. $\ln H$ as function of temperature and sulfuric acid concentration. The values in brackets were excluded from the linear fit

studies of thin sulfuric acid films by Middlebrook et al. (1993) who observed that film freezing occurred only below 200 K.

The temperature dependence of H is approximately given by

$$-\ln \frac{H}{H_0} = \frac{\Delta_s H}{R} \frac{1}{T} - \frac{\Delta_s S}{R}, \quad (8)$$

where $H_0 \equiv 1 \text{ mol kg}^{-1} \text{ bar}^{-1}$ is the standard Henry's law constant. Thus, by fitting straight lines through the data points in Fig. 2, enthalpies and entropies of solution can be determined for SO_2 in sulfuric acid solvents. The results are summarized in Table 1.

Because absorption and re-evaporation of SO_2 into and out of the sulfuric acid film is rate limited by diffusion in liquid solution, the SO_2 peaks are much broader than the SF_6 peaks, Fig. 1. In the theory of gas chromatography peak broadening is described by the number n of theoretical plates,

$$n = (t_r/\sigma)^2, \quad (9)$$

and the height equivalent of a theoretical plate

$$\text{HETP} = \frac{l}{n}. \quad (10)$$

Table 1

Enthalpy and entropy of solvation of SO₂ in sulfuric acid. Errors were calculated from the least squares fits. The data-points in brackets in Fig. 2 were excluded

$w(\text{H}_2\text{SO}_4)$	h	$\Delta_s H$	$\Delta_s S$
wt%	[μm]	[kJ mol ⁻¹]	[J K ⁻¹ mol ⁻¹]
0	–	-39.8 ± 0.1	-138.6 ± 2.6
41	1.2	-36.4 ± 1.2	-130.6 ± 5.2
62	1.5	-31.4 ± 0.3	-111.4 ± 1.2
83	2.1	-26.8 ± 0.2	-96.8 ± 0.8

The HETP is given as function of k' and the flow speed u by the Golay equation (Giddings 1991):

$$\text{HETP} = \frac{2D_g}{u} + \frac{(1 + 6k' + 11k'^2)}{96(k' + 1)^2} \frac{d^2}{D_g} u + \frac{2k'j}{3(k' + 1)^2} \frac{h^2}{D_l} u. \quad (11)$$

D_g and D_l are the diffusion coefficients of the solute in the gas and liquid phases. D_g for SO₂ in air was calculated using the following formula, which is based on a measurement of D_g by Andrew (1955) at ambient temperature:

$$D_g = 1.22 \times 10^{-5} \frac{\text{m}^2}{\text{s}} \left(\frac{1.013 \text{bar}}{p} \right) \left(\frac{T}{293 \text{K}} \right)^{1.75} \quad (12)$$

If the capacity ratio k' is small enough, as in the case of SO₂ in sulfuric acid films, peak broadening is mainly caused by liquid phase diffusion, and the first two terms of equation (11) are negligible. The liquid phase diffusion coefficients can thus be calculated from the second central moments of the SO₂ peaks applying equation (11) in combination with (9) and (10). A semilog plot of the obtained diffusion coefficients of SO₂ in sulfuric acid *versus* T is shown in Fig. 3. These values have to be regarded as lower limits, because film inhomogeneities will cause extra peak broadening.

In a simplistic model of large spherical solute molecules moving in a viscous solvent, the liquid diffusion coefficient of the solute should be given by the Stokes-Einstein relation, e.g. (Atkins 1986),

$$D_l = \frac{kT}{6\pi\eta a} \quad (13)$$

where a is called the hydrodynamic radius of the solute, i.e. the effective radius of the molecule *including* its strongly bound solvation shell(s). Using

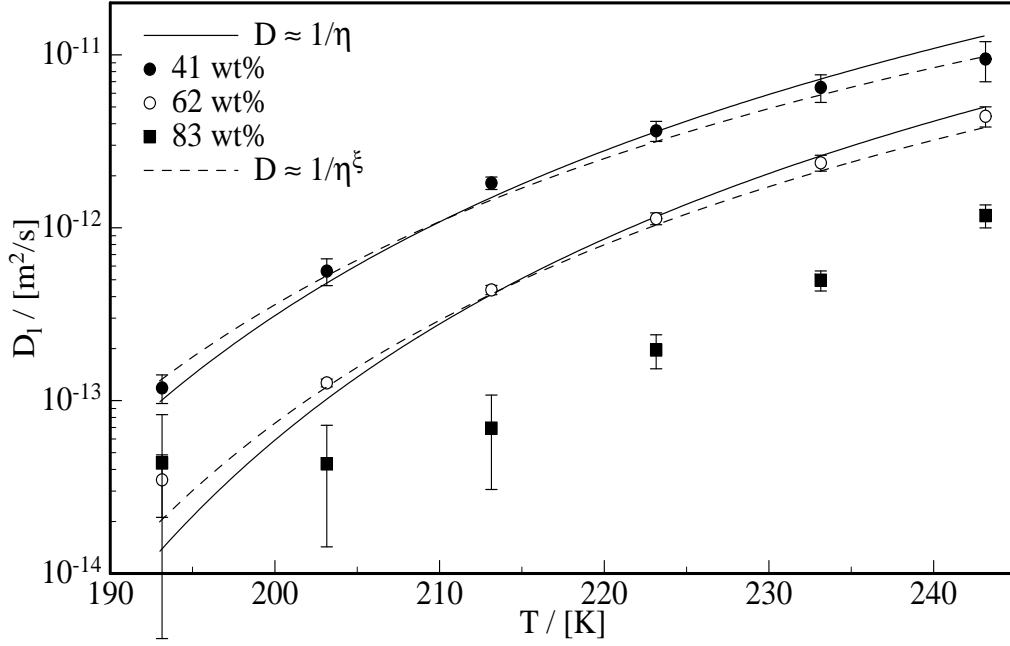


Fig. 3. Calculated diffusion coefficients from the second central moments of the SO_2 peaks. The solid curve is based on equation (13) and mean hydrodynamic radii of 1.14 nm for 41wt% and 0.84 nm for 62wt%. The dashed curves are based on equation (14) and the parameters given in the text

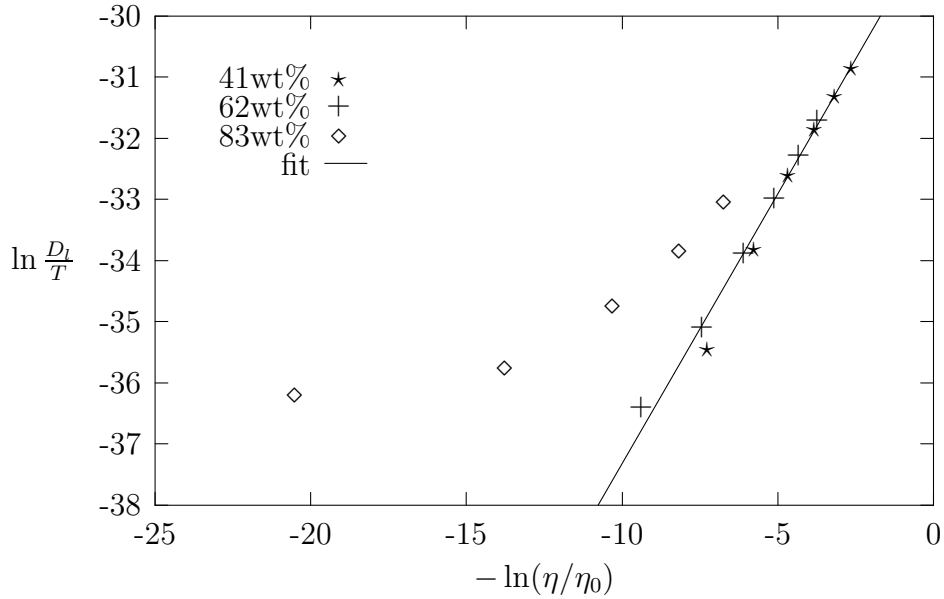


Fig. 4. Logarithmic plot of D_1/T vs. $\eta(T, w)$ to determine the parameters a_0 and ξ of equation (14)

parameterized viscosity data for cold sulfuric acid solutions from recent work of Williams and Long (1995), the validity of equation (13) could be tested. The solid lines in Fig. 3 were obtained by fitting equation (13) to the data, assuming constant mean hydrodynamic radii for each sulfuric acid concentration. Clearly the fits are not good, indicating that the apparent hydrodynamic radius of SO_2

is a function of temperature and acid concentration.

Heuberger and Sillescu (1996) have tested the validity of equation (13) for several photochromic tracers in glass forming organic liquids close to the glass forming temperature. They found that, for tracer molecules smaller than the solvent, the temperature dependence of D_l can be approximated by $D_l \propto T/\eta(T)^\xi$ with a constant exponent $\xi < 1$, and proposed the following modified Stokes-Einstein equation:

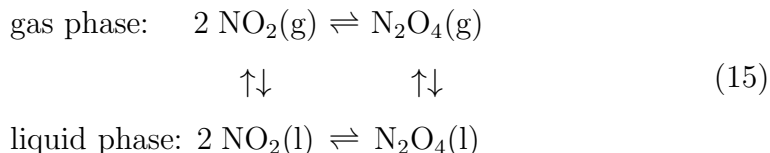
$$D_l = \frac{kT}{6\pi\eta_0(\eta/\eta_0)^\xi a_0}. \quad (14)$$

If this relation is valid, a plot of $\ln(D_l/T)$ vs. $-\ln(\eta/\eta_0)$ ($\eta_0 = 1$ cP) should yield a straight line. This is confirmed in Fig. 4 for the diffusion of SO_2 in 41wt% and 62wt% H_2SO_4 . The fit fails, however, for 83wt% sulfuric acid, probably because the viscosity data used in the fit, which had to be extrapolated to low temperatures and high acid concentrations, were in error. The parameters of the linear fits are $\xi = 0.88 \pm 0.03$ and $a_0 = (1.7 \pm 0.3)$ nm. This is much larger than the collision radius of 0.2 nm in the gas phase, based on viscosity data of gaseous SO_2 (Reid et al. 1987).

3.2 Solubilities of NO_2 and N_2O_4

As shown in Fig. 5, injections of increasing amounts of NO_2 give rise to increasing peak areas, indicating that no fast irreversible losses of NO_2 occur on the experimental time scale. However, in sharp contrast to the SO_2 peaks in Fig. 1, NO_2 peak shapes are distinctly non-Gaussian. Particularly at low temperatures and for large injected amounts of NO_2 the peaks take on a triangular shape, superimposed by strong tailing. Increasing the injected amounts of NO_2 resulted in systematic shifts of the peak maxima to longer “retention”-times.

An interpretation of the observed peak shapes can be given if we assume for the moment that consecutive chemical reactions in cold sulfuric acid solutions are negligible on the experimental time scale: NO_2 dimerizes in the gas and liquid phases to form N_2O_4 . Both the monomer and the dimer can individually dissolve in the acid film:



Dimer (N_2O_4) formation is favoured (a) by decreasing the temperature, (b) by

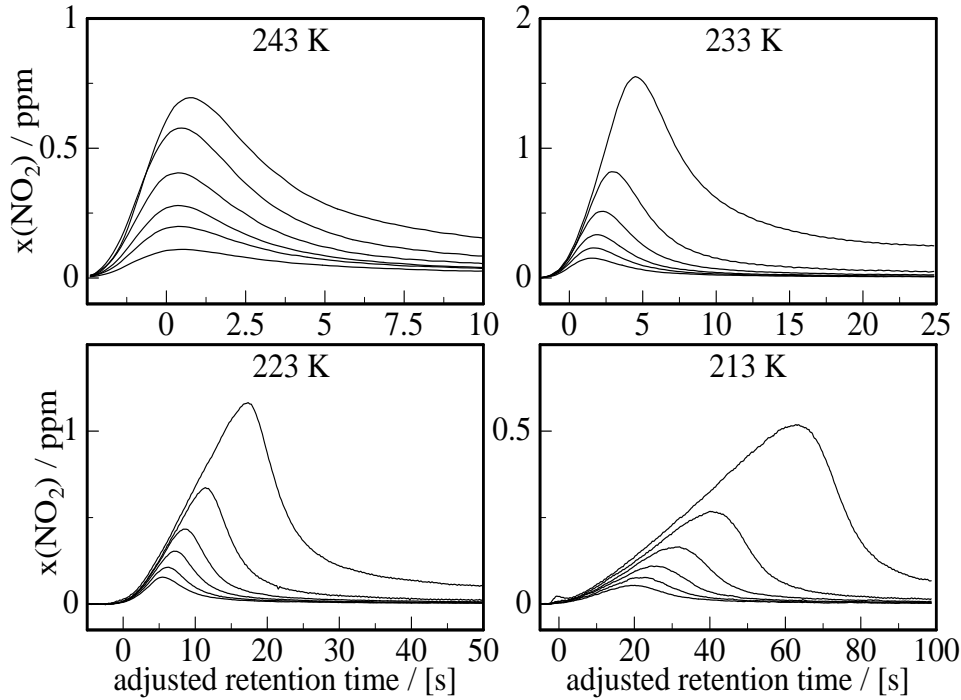


Fig. 5. Chromatograms of NO_2 on 59wt% H_2SO_4 , flow-rate 20 ml min^{-1} . These peaks were generated by injecting $100 \mu\text{l}$ of NO_2 in the range 9-94 ppm

increasing the NO_2 concentration. Thus, because peak maxima appear later when more NO_2 is injected, the solubility of N_2O_4 must be significantly larger than the solubility of the monomer, NO_2 . This is in qualitative agreement with the solubility ratio of the dimer and the monomer in aqueous solution (Schwartz and White 1981).

The dissociation-association constant of NO_2 in the gas phase is given by

$$K_p = \frac{p^2(\text{NO}_2)}{p(\text{N}_2\text{O}_4)p^0} \quad (16)$$

where $p^0 = 1 \text{ bar}$ is the standard pressure. The temperature dependence of K_p , based on experimental data of Harwood and Jones (1994), is given by

$$\ln K_p = -6572.7/T + 19.96. \quad (17)$$

This expression is believed to yield K_p values with an error of about 10%.

For the interpretation of the peak shapes it is assumed that the equilibria (15) in both phases are always established on the relevant experimental time scale. Instead of dealing with NO_2 and N_2O_4 separately, the pseudo species $\text{N}_{\text{IV}} = \text{NO}_2 + 2 \text{N}_2\text{O}_4$ is considered. Because the absorption isotherm of N_{IV} is nonlinear, the theory of chromatography has to be modified accordingly. Thus

Table 2

Solubilities of NO₂ and N₂O₄ depending on temperature and concentration. The indicated errors are obtained from the fit

w	h	T	$H(\text{NO}_2)$	$H(\text{N}_2\text{O}_4)$
wt%	[μm]	[K]	[mol kg ⁻¹ bar ⁻¹]	[mol kg ⁻¹ bar ⁻¹]
39	2.1	243	0.5 ± 0.1	98 ± 10
		233	2.6 ± 0.1	154 ± 4
		223	7.7 ± 0.3	351 ± 7
		213	25 ± 3	1076 ± 47
		203	50 ± 7	4530 ± 162
59	1.1	243	1.4 ± 0.5	347 ± 139
		233	3.1 ± 0.1	252 ± 10
		223	6.9 ± 0.3	417 ± 10
		213	21.1 ± 0.8	951 ± 21
		203	65 ± 4	3335 ± 104
68	1.6	243	0.5 ± 0.2	–
		233	1.4 ± 0.2	33 ± 8
		223	4.7 ± 0.2	77 ± 3
		213	11.2 ± 0.6	207 ± 6
		203	37 ± 6	496 ± 31

Table 3

Enthalpy and entropy of solvation of NO₂ and N₂O₄ in sulfuric acid. The error ranges are determined from the linear fit

	w	$\Delta_s H$	$\Delta_s S$
	wt%	[kJ mol ⁻¹]	[J K ⁻¹ mol ⁻¹]
NO ₂	59	-39.9 ± 0.8	-162 ± 4
NO ₂	68	-38.5 ± 0.2	-160 ± 8
N ₂ O ₄	68	-36.0 ± 2.0	-125 ± 10

the definition of the capacity ratio k' according to equation (5) was generalized as follows (Huber and Gerritse 1971):

$$k' = \left(\frac{\partial n_l(\text{N}_{\text{IV}})}{\partial n_g(\text{N}_{\text{IV}})} \right)_z. \quad (18)$$

z is the coordinate along the column axis. When the N_{IV} peak passes the

column, the amounts n_g and n_l of N_{IV} in the gas and liquid phases in each short section Δz of the column are given by the following equations:

$$\begin{aligned} n_g(N_{IV}) &= \frac{\pi r^2 \Delta z}{RT} [p(\text{NO}_2) + 2p(\text{N}_2\text{O}_4)] \\ &= \frac{\pi r^2 \Delta z}{RT} p(N_{IV}); \end{aligned} \quad (19)$$

$$\begin{aligned} n_l(N_{IV}) &= (m_l/l)\Delta z [H(\text{NO}_2)p(\text{NO}_2) + 2H(\text{N}_2\text{O}_4)p(\text{N}_2\text{O}_4)] \\ &= (m_l/l)\Delta z \left\{ \frac{H(\text{NO}_2)K_p p^0}{4} \left[\sqrt{1 + \frac{8p(N_{IV})}{K_p p^0}} - 1 \right] \right. \end{aligned} \quad (20)$$

$$\left. + 2H(\text{N}_2\text{O}_4) \left[\frac{p(N_{IV})}{2} - \frac{K_p p^0}{8} \left(\sqrt{1 + \frac{8p(N_{IV})}{K_p p^0}} - 1 \right) \right] \right\} \quad (21)$$

Combining these expressions with equation (18) yields the capacity ratio of the pseudo species N_{IV} as function of its mixing ratio $x(N_{IV})$:

$$k' = \frac{m_l RT}{\pi r^2 l} \frac{H(\text{NO}_2) + H(\text{N}_2\text{O}_4) \left(\sqrt{1 + \frac{8x(N_{IV})p_0}{K_p p^0}} - 1 \right)}{\sqrt{1 + \frac{8x(N_{IV})p_0}{K_p p^0}}} \quad (22)$$

(note that p_0 is the pressure at column exit, while p^0 is the standard pressure of 1 bar.)

For further analysis the *peak maxima method* (Huber and Gerritse 1971) is used. In order to determine the solubilities $H(\text{NO}_2)$ and $H(\text{N}_2\text{O}_4)$, it is assumed that equation (22) applies to the peak maxima, i.e. that the first part of equation (5) can be used with $t_r(N_{IV}) =$ position of the peak maximum to calculate the capacity ratio k' of the pseudo species N_{IV} . Then the solubilities $H(\text{NO}_2)$ and $H(\text{N}_2\text{O}_4)$ are determined by fitting equation (22) to a series of chromatograms with different mixing ratios $x(N_{IV})$ at the positions of the peak maxima, as shown in Fig. 6. The obtained solubilities are summarized in Table 2. For a semilog plot see Fig. 7. An approximate error of 20% is estimated for $H(\text{NO}_2)$, arising mainly from the uncertainty of the nonlinear fit. The estimated error of 30% for $H(\text{N}_2\text{O}_4)$ is somewhat larger because the uncertainty in K_p , see above, must also be included. Semilog plots of H/H_0 versus $1/T$ for NO_2 and N_2O_4 are shown in Fig. 7. In cases where the fits are approximately linear enthalpies and entropies of solution are determined which are listed in Table 3.

The consistency of the *peak maxima method* was checked by theoretical peak

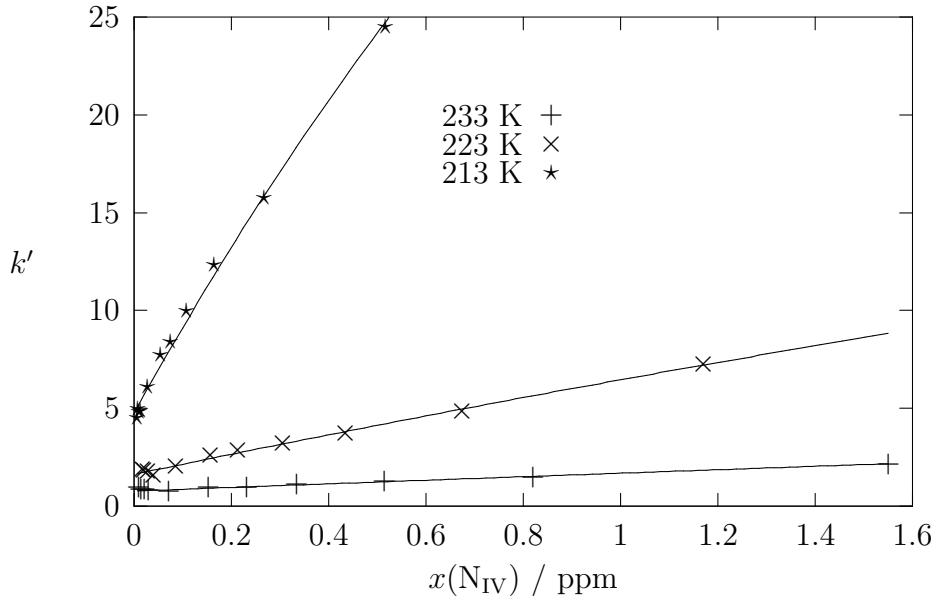


Fig. 6. Nonlinear fit of equation (22) to the locations of the experimental peak maxima for 59wt% H_2SO_4

shape calculations. On the basis of plate theory the column can be described as a series of ideal phase mixers (Yamaoka and Nakagawa 1975). The mass balance in each mixer is given by

$$\frac{dc_i}{dt} = \frac{c_{i-1} - c_i}{\tau} \frac{1}{1 + k'(c_i)}. \quad (23)$$

τ is the residence time of the carrier gas in each phase mixer. c_i is the concentration of the pseudo species N_{IV} in the i -th mixer. k' is calculated using equation (22). The total number of ideal mixers representing the column is varied until a good fit of the observed peak shape is obtained. The solubilities determined by the peak maxima method were used as input parameters to peak shape calculations. Originals and simulated peaks are compared in Fig. 8. The qualitative agreement is rather good, if one disregards additional tailing effects which cannot be reproduced by the simple plate theory. However, retention times of $x(\text{N}_{\text{IV}})$ are somewhat underpredicted by the simulations, implying that the solubilities $H(\text{N}_2\text{O}_4)$ determined by the peak maxima method must be regarded as lower limits.

At this point we have to justify our assumption that the possible reactions (1) and (2) need not be taken into account in these calculations. As shown in the Appendix, the equilibrium constants of both reactions can be calculated from measurements and literature data. In less concentrated sulfuric acid solutions the conversion of 2 NO_2 or N_2O_4 into HONO and HNO_3 *via* reaction (1) is favoured. In more concentrated sulfuric acid NO^+ and HNO_3 are the preferred products. The solubilities of these products in cold sulfuric acid are rather high, so any NO_2 removed by reactions (1) and (2) would be missing in the

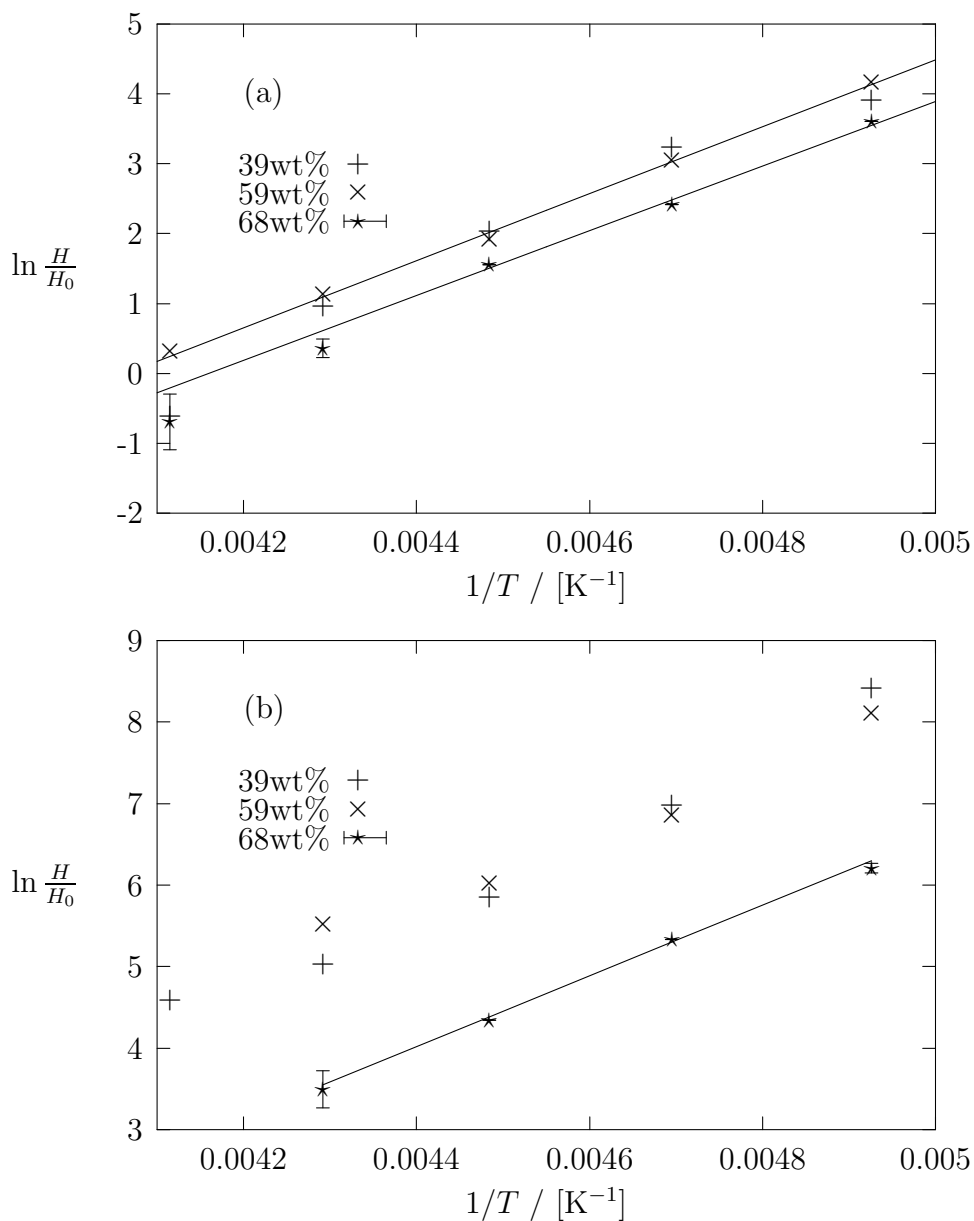


Fig. 7. (a) semilogarithmic plot of solubilities of NO_2 . The lines are the fits for 59wt% and 68wt%. (b) solubilities of N_2O_4 .

recovered NO_2 peak area. The recovered fractions of NO_2 were determined by integrating peak areas, although this was somewhat ambiguous because of the peak tailing. The integrations yielded up to 40% NO_2 lost on sulfuric acid. Assuming a first order loss process of NO_2 in the column, this corresponds to a reaction coefficient (Hu et al. 1995) $\gamma \leq 7 \times 10^{-7}$.

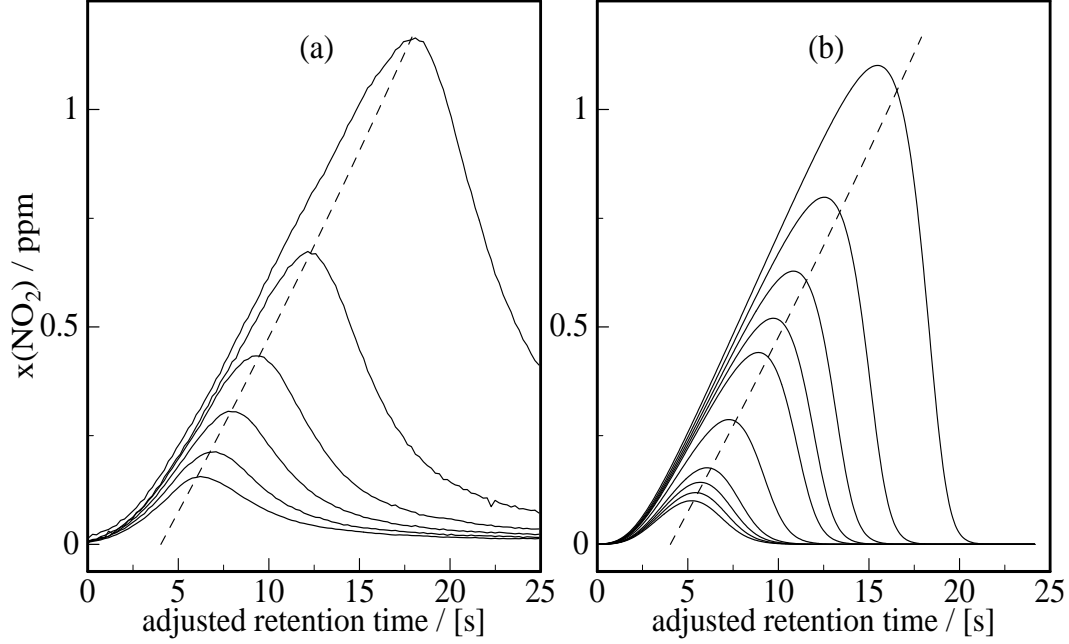


Fig. 8. Comparison of (a) experimental and (b) simulated peak-shapes at 223 K and 59wt%. The number of mixers is 20. The NO_2 injection concentrations are 11.4, 15.1, 21.8, 36.4, 94.0 ppm for the experimental peaks and 1.4, 1.7, 2.1, 2.7, 5.0, 9.0, 11.4, 15.1, 21.8, 36.4 ppm for the simulated peaks. The dashed lines are calculated with equation (22). They represent the locations of the experimental peak maxima

4 Atmospheric Implications

For less soluble compounds phase equilibrium between droplet aerosols and interstitial air is rapidly established. The phase ratio of a species i which is present in the gas phase with a mixing ratio x_i and is only physically absorbed in sulfuric acid droplets is given by

$$\left(\frac{n_l}{n_g}\right)_i = H_i RT \rho_{\text{acid}} L. \quad (24)$$

(note that H for sulfuric acid is given in units of $[\text{mol kg}^{-1} \text{bar}^{-1}]$). L is the volume fraction occupied by the liquid droplet aerosol. A typical value for a dense Pinatubo aerosol would be $L = 3 \times 10^{-12}$ (Hanson et al. 1994). If this aerosol consists of 83wt% supercooled sulfuric acid droplets at 200 K, the phase ratio of SO_2 would be about 10^{-8} . Hence, absorption of SO_2 in sulfuric acid aerosol will be totally negligible in the upper troposphere and lower stratosphere.

Since the lifetime of NO_2 with respect to its reaction with OH is about 0.4 days in the upper troposphere (Arnold et al. 1992), possible reactions of NO_2 in sulfuric acid droplets would have to be extremely fast to compensate for

its low solubility. Our observation that reactions (1) and (2) of NO_2 are slow in sulfuric acid under upper tropospheric / lower stratospheric conditions is consistent with results of Saastad et al. (1993), who report an upper limit of 5×10^{-5} for the uptake coefficient of NO_2 . Hence, the reaction of NO_2 with sulfuric acid droplets is not considered to be an important source of HONO, or of nitrosyl cations, at aircraft cruising height.

5 Conclusion

We have shown that solubilities and diffusion coefficients of trace gases in cold sulfuric acid solutions can be measured in the range of mid tropospheric to stratospheric temperatures, using sulfuric acid coated capillary columns and suitable trace gas detectors to determine capacity ratios and peak shapes. The method was applied to SO_2 and to NO_2 in equilibrium with its dimer N_2O_4 . Limited information on the reactivity of NO_2 in cold sulfuric acid could also be obtained. For the compounds studied it was found that interactions with sulfuric acid aerosols are negligible at aircraft cruising height.

Acknowledgement

This work is supported by the “Deutsche Forschungsgemeinschaft (DFG)” within the DFG-priority programme “Basics of the Impact of Air and Space Transportation on the Atmosphere”.

References

- Andrew, S. (1955). A simple method of measuring gaseous diffusion coefficients. *Chem. Eng. Sci.* **4**, 269–272.
- Arnold, F., Scheid, J., and Stilp, T. (1992). Measurements of jet aircraft emissions at cruise altitude I: The odd-nitrogen gases NO , NO_2 , HNO_2 and HNO_3 . *Geophys. Res. Lett.* **12**, 2421–2424.
- Atkins, P. (1986). *Physical Chemistry*. Oxford University Press.
- Becker, K., Kleffmann, J., Kurtenbach, R., and Wiesen, P. (1996). Solubility of nitrous acid (HONO) in sulfuric acid solutions. *J. Phys. Chem.* **100**, 14984–14990.
- Bongartz, A., Kames, J., Welter, F., and Schurath, U. (1991). Near-UV absorption cross sections and cis/trans equilibrium of nitrous acid. *J. Phys. Chem.* **95**, 1076–1082.

- Carslaw, K., Clegg, S., and Brimblecombe, P. (1995). A thermodynamic model of the system HCl-HNO₃-H₂SO₄-H₂O, including solubilities of HBr from < 200 to 328 K. *J. Phys. Chem.* **99**, 11557–11574.
- Chase, M., Davies, C., Downey, J., Frurip, D., McDonald, R., and Syverud, A. (1985). JANAF Thermochemical Tables. In *J. Phys. Chem. Ref. Data* (3 ed.), Volume 14, Supplement 1.
- Fenter, F. and Rossi, M. (1996). Heterogeneous kinetics of HONO on H₂SO₄ solutions and on ice: Activation of HCl. *J. Phys. Chem.* **100**, 13765–13775.
- Gable, C., Betz, H., and Maron, S. (1950). Phase equilibria of the system sulfur trioxide-water. *J. Am. Chem. Soc.* **72**, 1445–1448.
- Giddings, J. (1991). *Unified Separation Science*. Wiley.
- Goldberg, R. and Parker, V. (1985). Thermodynamics of solution of SO₂(g) in water and of aqueous sulfur dioxide solutions. *J. Res. Natl. Bur. Stand. (U.S.)* **90**, 341–358.
- Goodman, K. and Brenna, J. (1994). Curve fitting for restoration of accuracy for overlapping peaks in gas chromatography/combustion isotope ratio mass spectrometry. *Anal. Chem.* **66**, 1294–1301.
- Guiochon, G. (1971). Prediction of the average film thickness in capillary columns prepared by the dynamic method. *J. Chrom. Sci.* **9**, 512.
- Hanson, D., Ravishankara, A., and Solomon, S. (1994). Heterogeneous reactions in sulfuric acid aerosols: A framework for model calculations. *J. Geophys. Res.* **99**, 3615–3629.
- Harwood, M. and Jones, R. (1994). Temperature dependent ultraviolet-visible absorption cross sections of NO₂ and N₂O₄: Low-temperature measurements of the equilibrium constant for 2 NO₂ ⇌ N₂O₄. *J. Geophys. Res.* **99**, 22955–22964.
- Heuberger, G. and Sillescu, H. (1996). Size dependence of tracer diffusion in supercooled liquids. *J. Phys. Chem.* **100**, 15255–15260.
- Hu, J., Shi, Q., Davidovits, P., Worsnop, D., Zahniser, M., and Kolb, C. (1995). Reactive uptake of Cl₂(g) and Br₂(g) by aqueous surfaces as a function of Br⁻ and Cl⁻ concentration: The effect of chemical reaction at the interface. *J. Phys. Chem.* **99**, 8768.
- Huber, J. and Gerritse, R. (1971). Evaluation of dynamic gas-chromatographic methods for the determination of adsorption and solution isotherms. *J. Chromatogr.* **58**, 137.
- Kärcher, B. (1996). Aircraft-generated aerosols and visible contrails. *Geophys. Res. Lett.* **23**, 1933–1936.
- Kärcher, B., Peter, T., Biermann, U., and Schumann, U. (1996). The initial composition of jet condensation trails. *J. Atmos. Sci.* **53**, 3066–3083.
- Kärcher, B., Peter, T., and Ottmann, R. (1995). Contrail formation: Homogeneous nucleation of H₂SO₄/H₂O droplets. *Geophys. Res. Lett.* **22**, 1501–1504.
- Middlebrook, A., Iraci, L., McNeill, L., Koehler, B., Wilson, M., Saastad, O., Tolbert, M., and Hanson, D. (1993). Fourier transform-infrared stud-

- ies of thin $\text{H}_2\text{SO}_4/\text{H}_2\text{O}$ films: Formation, water uptake, and solid-liquid phase changes. *J. Geophys. Res.* **98**, 20473–20481.
- Nyarady, S., Barkley, R., and Sievers, R. (1985). Redox chemiluminescence detector: Application to gas chromatography. *Anal. Chem.* **57**, 2074–2079.
- Redant, G., Sandra, P., and Verzele, M. (1982). Some observations on dynamic coating of capillary columns. *Chromatographia* **15**, 13.
- Reid, R., Prausnitz, J., and Poling, B. (1987). *The Properties of Gases and Liquids* (4 ed.). New York: McGraw-Hill.
- Saastad, O., Ellermann, T., and Nielsen, C. (1993). On the adsorption of NO and NO_2 on cold $\text{H}_2\text{O}/\text{H}_2\text{SO}_4$ surfaces. *Geophys. Res. Lett.* **20**, 1191–1193.
- Sabinina, L. and Terpugow, L. (1935). Die Oberflächenspannung des Systems Schwefelsäure-Wasser. *Z. Physikal. Chemie* **A173**, 237–241.
- Schumann, U., Ström, J., Busen, R., Bamann, R., Gierens, K., Krautstrunk, M., Schröder, F., and Stingl, J. (1996). In situ observations of particles in jet aircraft exhaust and contrails for different sulfur-containing fuels. *J. Geophys. Res.* **101**, 6853–6869.
- Schwartz, S. and White, W. (1981). Solubility equilibria of the nitrogen oxides and oxoacids in dilute aqueous solution. *Adv. Environ. Sci. Technol.* **4**, 1–45.
- Taleb, D., Ponche, J., and Mirabel, P. (1996). Vapor pressures in the ternary system water-nitric acid-sulfuric acid at low temperature: A reexamination. *J. Geophys. Res.* **101**, 25967–25977.
- Wiesen, P., Kleffmann, J., Kurtenbach, R., and Becker, K. (1995). Mechanistic study of the heterogeneous conversion of NO_2 into HONO and N_2O on acid surfaces. *Faraday Discuss.* **100**, 121–127.
- Williams, L. and Long, F. (1995). Viscosity of supercooled sulfuric acid solutions. *J. Phys. Chem.* **99**, 3748–3751.
- Yamaoka, K. and Nakagawa, T. (1975). Moment analysis of non-linear gas chromatography by computer simulation. *J. Chromatogr.* **103**, 221–227.
- Zhang, R., Leu, M., and Keyser, L. (1996). Heterogeneous chemistry of HONO on liquid sulfuric acid: A new mechanism of chlorine activation on stratospheric sulfate aerosols. *J. Phys. Chem.* **100**, 339–345.
- Zhang, R., Wooldridge, P., and Molina, M. (1993). Vapor pressure measurement for the $\text{H}_2\text{SO}_4/\text{HNO}_3/\text{H}_2\text{O}$ and $\text{H}_2\text{SO}_4/\text{HCl}/\text{H}_2\text{O}$ systems: Incorporation of stratospheric acids into background sulfate aerosols. *J. Phys. Chem.* **97**, 8541–8548.

A Liquid phase equilibria of NO₂

The liquid phase equilibrium constant of reaction (1) is expressed in molalities b :

$$K_{1,l}(w, T) = \frac{b(\text{HNO}_3)b(\text{HONO})}{b^2(\text{NO}_2)}. \quad (\text{A.1})$$

Since the solubilities of all components are known, $K_{1,l}(w, T)$ can be calculated from the gas-phase equilibrium constant:

$$\begin{aligned} K_{1,g} &= \frac{p(\text{HNO}_3)}{p^2(\text{NO}_2)p(\text{H}_2\text{O})} [p(\text{cis-HONO}) + p(\text{trans-HONO})] \\ &= K_{1,g}(\text{cis-HONO}) + K_{1,g}(\text{trans-HONO}). \end{aligned} \quad (\text{A.2})$$

The relation between the equilibrium constants is

$$K_{1,l} = \frac{H(\text{HNO}_3)H(\text{HONO})}{H^2(\text{NO}_2)} p(\text{H}_2\text{O})K_{1,g}. \quad (\text{A.3})$$

With thermochemical constants of Chase et al. (1985), $K_{1,g}$ is given by the equation

$$\ln K_{1,g} = \frac{4200.6\text{K}}{T} - 17.026 - 0.779 \ln \left(\frac{T}{298.15\text{K}} \right) \quad (\text{A.4})$$

in the range $T = 198 - 298$ K. The effective solubility of HNO₃ can be calculated from vapour pressure measurements of Zhang et al. (1993), who report the following parameterisation for the range $T = 190 - 230$ K and $w(\text{H}_2\text{SO}_4) = 35 - 75$ wt%:

$$\begin{aligned} \lg p(\text{HNO}_3) &= \lg w(\text{HNO}_3) + a_1(T) + a_2(T)w(\text{H}_2\text{SO}_4) \\ &\quad + a_3(T)w(\text{HNO}_3) \end{aligned} \quad (\text{A.5})$$

with

$$a_i = A_i + \frac{B_i}{T}.$$

With $b(\text{HNO}_3) = w(\text{HNO}_3)/M(\text{HNO}_3)$ and

$$H(\text{HNO}_3) = \lim_{p \rightarrow 0} \left(\frac{\partial b(\text{HNO}_3)}{\partial p(\text{HNO}_3)} \right) \quad (\text{A.6})$$

the effective solubility is given by

$$\ln \frac{H(\text{HNO}_3)}{H_0} = \frac{8497 - 2395w}{T} - 12.84 - 6.724w. \quad (\text{A.7})$$

An expression for the physical solubility of HONO and the proton activity dependent equilibrium constant of reaction (2) is derived from the solubility data parameterisation of Becker et al. (1996). The effective solubility

$$H_{\text{eff}}(\text{HONO}) = \frac{b(\text{HONO}) + b(\text{NO}^+)}{p(\text{HONO})} \quad (\text{A.8})$$

$$H_{\text{eff}}(\text{HONO}) = H(\text{HONO}) + H(\text{HONO})K_{2,l} \quad (\text{A.9})$$

is expressed as

$$H_{\text{eff}}(\text{HONO}) = A \exp(100Bw) + D \exp(100Ew) \quad (\text{A.10})$$

The first term of equation (A.10) corresponds to the first term of equation (A.9), the second term of equation (A.10) to the second term of equation (A.9). In the range $T = 248 - 298$ K and $w(\text{H}_2\text{SO}_4) = 0 - 67\text{wt}\%$ the solubility is given by

$$\ln \frac{H(\text{HONO})}{H_0} = \frac{4873 + 1286w}{T} - 12.45 - 9.15w \quad (\text{A.11})$$

and the equilibrium constant of reaction (2) is given by

$$\ln K_{2,l} = \frac{3029 - 4855w}{T} - 42.24 + 73.13w \quad (\text{A.12})$$

At 243 K $K_{1,g} = 1.52 \text{ bar}^{-1}$ is obtained. In 39wt% sulfuric acid the equilibrium constant is $K_{1,l} = 4.3 \times 10^6$, using equation (A.3), $H(\text{NO}_2) = 0.5 \text{ mol kg}^{-1}\text{bar}^{-1}$, $p(\text{H}_2\text{O}) = 2.5 \times 10^{-4} \text{ bar}$ (Taleb et al. 1996) and the solubilities calculated with equations (A.7) and (A.11). Therefore the equilibrium ratio is $b(\text{HNO}_3)/b(\text{NO}_2) = 2.1 \times 10^3$. With increasing sulfuric acid concentration, $K_{1,l}$ decreases to 6.5×10^2 at 68wt%, but $K_{2,l}$ increases from 1.2×10^{-4} at 39wt% to 583 at 68wt%.